Journal of Applied Electrochemistry **32**: 1131–1140, 2002.

Oxygen reduction on silver catalysts in solutions containing various concentrations of sodium hydroxide – comparison with platinum

M. CHATENET[1,*], L. GENIES-BULTEL[1], M. AUROUSSEAU[1], R. DURAND[1] and F. ANDOLFATTO[2]
[1]*Laboratoire d'Electrochimie et de Physicochimie des Matériaux et des Interfaces (LEPMI, UMR 5631 CNRS-INP Grenoble associated to the UJF), ENSEEG, BP 75, 38402 Saint Martin d'Hères Cedex, France*
[2]*Centre de Recherches Rhône-Alpes, ATOFINA, BP 63, rue H. Moissan, 69493 Pierre-Bénite Cedex, France*
*(*author for correspondence, e-mail: Marian.Chatenet@lepmi.inpg.fr)*

Received 26 July 2001; accepted in revised form 19 June 2002

Key words: high concentration, oxygen reduction, platinum, silver, sodium hydroxide

Abstract

In air cathodes for chlorine–sodium hydroxide production, silver is a suitable catalyst for the oxygen reduction reaction (ORR), as is platinum. The ORR mechanism, studied with both rotating disc and ring-disc electrodes and impedance spectroscopy, is first order towards O_2. However, the reaction can involve a direct four-electron or two-electron pathway. Although the latter involves different chemistry, including decomposition of hydrogen peroxide, the two pathways are difficult to distinguish, probably because they have the same rate-determining step. Considering kinetics/solubility ratios, temperature increase favours the ORR kinetics on both metals, whereas an increase in sodium hydroxide concentration is only positive for silver: for high sodium hydroxide concentration, platinum properties are hindered by greater adsorbed oxygenated species coverage. Thus, silver becomes competitive to platinum in high concentration alkaline media.

1. Introduction

Chlorine and sodium hydroxide production via membrane brine electrolysis involves high-energy consumption. Replacing the hydrogen evolution cathode by an air cathode would lead to a large cell voltage decrease (1.23 V on the open-circuit voltage) and thus to energy savings. Such savings depend on the use of highly dispersed catalysts for the oxygen reduction reaction (ORR) in the gas diffusion electrode to minimize overpotential. In dilute alkaline electrolytes, carbon-supported nanoparticles such as Pt/C [1–3] or Ag/C [4, 5] have been used in view of their high specific area and good catalytic activity [6]. Studies with high concentration sodium hydroxide solutions, for either Pt/C [7–10] or Ag/C [11], are scarce and do not generally deal with the ORR mechanism and kinetics in industrial conditions (11.1 M NaOH at 80 °C). The present work determines the kinetic parameters and mechanisms for this reaction on Ag/C and Pt/C in 11.1 M sodium hydroxide at 80 °C. Operating conditions, such as the solution temperature, sodium hydroxide concentration and oxygen partial pressure, which affect the catalyst behaviour are studied, as are aspects of mechanism; the number of electrons exchanged per oxygen molecule is determined and several variants for the ORR mechanism are proposed.

2. Experimental procedures

2.1. *Apparatus and solutions*

Rotating disc electrode (EDT 101, Tacussel) experiments were carried out using both silver and platinum catalysts, either as bulk polycrystalline materials (noted as Ag and Pt) or as carbon-supported nanoparticles (noted as Ag/C and Pt/C). These supported materials were 10 wt % Ag on Vulcan XC 72 (Cabot) and 10 wt % Pt/C from E-Tek, the latter being used without any additional electrochemical treatment. The nanoparticle-based active layer was deposited on a glassy carbon electrode (dia. 5×10^{-3} m) previously polished with diamond paste to 10^{-6} m, and washed for 15 min in ultrasonic baths of acetone, ethanol–water (1–1) and water successively. The resulting layer (2.6×10^{-6} m thick) was sintered for 15 min at 180 °C in an inert atmosphere. Bulk polycrystalline silver or platinum RDE were polished as described above. Oxygen reduction was studied in 0.1, 0.5 and 1 M (Normapur, Prolabo) and 11.1 M (Atofina) sodium hydroxide solutions. The latter solution was termed 'industrial solution' when held at 80 °C. The temperature (10, 25, 40 or 80 °C) was maintained by a RM6-Lauda water-circulation thermostat–cryostat; the room temperature was 25 °C.

Voltammetry experiments were made using a potentiostat PAR 263 (EG&G) with a three-electrode cell.

Impedance spectroscopy was performed with a Solartron system (1255 and 1287).

2.2. *Silver based catalyst (Ag/C) preparation*

2.2.1. *Synthesis and deposition on the electrode*

Carbon powder (Vulcan XC 72, Cabot) was thermally activated for 1 h at 930 °C under a CO_2 atmosphere until a 26% mass loss was reached. Such heat-treatment enables partial cleaning of the carbon surface of its impurities and leads to moderate surface oxygenated species coverage; it also opens up microporosity, via carbon consumption [12, 13]. Such activated carbon was then impregnated with an $AgNO_3$ (Prolabo) solution in ultrapure (Millipore) water, leading to 10 wt % silver loading ($m_{Ag}/[m_{Ag} + m_C] = 10\%$). The active layer precursor was a mixture composed of the $AgNO_3$-impregnated Vulcan with a PTFE (10 wt % PTFE loading) suspension in water–ethanol (3–1 in volume). After one hour in an ultrasonic bath, a calibrated drop (10^{-5} L) of the mixture was deposited on the RDE and dried in air before sintering.

Pt/C (E-Tek) was mixed with PTFE to obtain a suspension (10 wt % loading for both PTFE and platinum) in water–ethanol (3–1).

2.2.2. *Electrochemical reduction of the active layer*

The active layer with silver particles was electroreduced in molar sulfuric acid (suprapur, Merck) in an argon atmosphere at 25 °C in a three-electrode cell with a PTFE false bottom. The method consisted of various amperometric pulses: crystallites germinated during the first pulse (-0.2 A cm^{-2} for 0.1 s), and the particles grew during the following (-5×10^{-2} A cm^{-2} for 1 s). Eight of these latter pulses were generally needed to achieve entire silver salt reduction. Then, ten 0.1 V s^{-1} voltammetric cycles (+0.3 to -0.88 V vs Hg/HgO) in alkaline solution were applied to clean the catalyst surface. This purification was controlled for each electrolyte by benchmark voltammograms at 10^{-2} V s^{-1} in the same potential range.

2.3. *Oxygen reduction quasi-steady-state voltammetry experiments*

Oxygen reduction voltammetry experiments were performed after electrode surface cleaning and characterization. During all the experiments, the oxygen concentration was kept constant at its saturation value by permanent O_2-bubbling. The quasi-steady-state voltammograms were recorded at 10^{-3} V s^{-1} from 0.1 to -0.6 V vs Hg/HgO in dilute sodium hydroxide solutions and from 0.04 to -0.6 V vs Hg/HgO in *industrial* (11.1 M) sodium hydroxide solution. The RDE rotation speed varied in the range 42–420 rad s^{-1} depending on the experiments. Prior to each voltammetry experiment, the potential was kept for one minute at the starting potential, 0.04 or 0.1 V vs Hg/HgO according to the sodium hydroxide concentration, to ensure an identical initial surface state in all experiments for a given solution.

In an *industrial* electrolyte, the very low oxygen solubility and corresponding oxygen reduction current render the current related to the surface oxygenated species reduction non-negligible, in contrast to a dilute electrolyte. Thus, this latter current (obtained in an inert atmosphere) was subtracted from the ORR current (in an O_2 atmosphere) in high concentration sodium hydroxide [14].

As in an acidic medium, the ORR overpotential (absolute value) exceeded 0.3 V in alkaline media for industrial current densities (about 3×10^3 A m^{-2}). Thus, from a kinetic point of view, the exchange current density i_0 is not so interesting: a small error in the determination of b_1 (Tafel slope for low overpotentials) would dramatically affect the i_0 determination. The current density measured at a conventional oxygen reduction potential: -0.1 V vs Hg/HgO, noted as i_{-100}, is more representative of the ORR kinetics. This potential corresponds to an ORR overpotential, in molar sodium hydroxide at 25 °C, around 0.4 V at 3×10^3 A m^{-2}. Such an overpotential value is targeted in the brine electrolysis industry, since it corresponds to massive energy savings compared to the usual cathodic hydrogen evolution potential.

The current density values were related to the active area of platinum or silver. The former was determined from classical hydrogen adsorption voltammetry in acidic medium and in an inert atmosphere and the latter from transmission electron microscope (TEM) or atomic force microscope (AFM) measurements (for Ag/C and Ag, respectively). Besides, when compared for different media, i_{-100} and i_0 values should not depend on the dissolved oxygen concentration. Provided oxygen solubility varies very significantly with sodium hydroxide solution temperature and concentration [14, 15], all current density values are averaged from several reproducible runs. They are also corrected by the oxygen solubility in the considered medium and related to that in molar sodium hydroxide at 25 °C. Such correction hides the experimental difficulty, as it renders all current density values artificially higher than they are in actuality.

2.4. *Number of electrons exchanged per oxygen molecule*

The number of electrons exchanged per oxygen molecule, n, was determined on a rotating ring disc electrode (RRDE) in an industrial electrolyte (11.1 M NaOH at 80 °C) both for bulk polycrystalline (Pt) and carbon-supported (Pt/C) platinum, according to the method of Geniès et al. [1].

3. Results and discussion

3.1. *Silver and platinum particle size*

Determining the active area for silver electrodes was one key issue of this work. Hydrogen-adsorption voltam-

metry, a technique classically used to determine the platinum electroactive area, is not efficient for silver. Various other methods are, however, reported in the literature. Lead or thallium underpotential deposition has, for example, been carried out [16–19] on silver single crystal substrate. This technique, however, can hardly be used to determine the active area of carbon-supported silver, as the electrochemical results are already difficult to expound on bulk polycrystalline silver [20]. Kita et al. [21] and Orozco et al. [22] have unsuccessfully attempted to adsorb and electrooxidise carbon monoxide, due to a lack of reproducibility. Savinova et al. [23, 24] have measured the roughness of bulk polycrystalline silver electrodes estimating silver double layer capacitance (C_s), but such a technique is not adequate for Ag/C: the silver active area was much smaller than that of the carbon substrate, rendering C_s results unreliable. Nekrassova et al. [25] have also used this technique on silver thin films, but the C_s values only led to the film roughness estimation when the silver film surface was very smooth, again showing the difficulty of transposing the method to determine the Ag/C active area. Thus, for lack of an alternative, the Ag/C catalyst silver active area was determined using TEM imaging.

The TEM photograph of Figure 1 shows the general shape for carbon-supported silver nanoparticles. An estimation based on 10 photographs, showed that, except for the very scarce big nanoparticles (dia. around $(2–5) \times 10^{-8}$ m), the silver nanoparticles diameter was in the range $(5–10) \times 10^{-9}$ m. The particles were also satisfactorily dispersed over the carbon support: neither silver particle agglomerates nor silver particle-free carbon zones were observed. A silver nanoparticle mean diameter, $d_{mean} = 7.0 \times 10^{-9}$ m, was deduced and described, using the classical formula:

$$d_{mean} = \frac{\sum f_i d_i^3}{\sum f_i d_i^2}$$

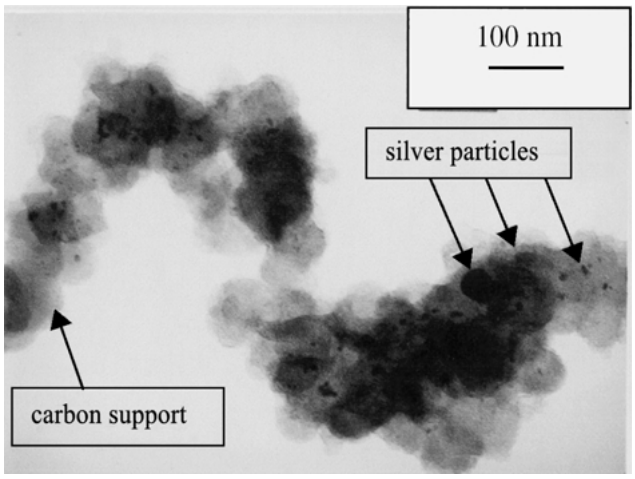

Fig. 1. TEM photograph for reduced carbon-supported silver nanoparticles.

f_i being the proportion of nanoparticles with diameter d_i.

The amount of silver in the active layer was known and led to 1.1×10^{-3} ($\pm 20\%$) m^2; as the active area of silver. For 1.96×10^{-5} m^2, the electrode geometric area, the roughness factor was 56 m^2 m^{-2}.

The commercial carbon-supported platinum nanoparticles (Pt/C, E-Tek) were fairly homogeneous in size, a mean diameter of $(2.0–2.5) \times 10^{-9}$ m was commonly accepted [1], and well dispersed over the carbon surface. The platinum particle mean diameter from hydrogen adsorption voltammetry and from TEM imaging were similar, respectively 2.4×10^{-9} m and 2.3×10^{-9} m, and in agreement with E-Tek data (2×10^{-9} m) [6]. The correlation between TEM values and the existing benchmarks validates the TEM use to determine the Ag/C active area.

3.2. *Bulk silver RDE roughness*

The bulk polycrystalline silver RDE atomic force microscope (AFM) characterization did not show differences compared to that of platinum after an identical polishing procedure. Now, as the roughness for polished-polycrystalline platinum, determined by hydrogen-adsorption coulometry in an inert atmosphere in ultrapure acidic medium [26], was close to 3, it will be assumed that polished polycrystalline silver also has a roughness close to 3.

3.3. *Influence of silver nanoparticle electrode pretreatment*

Literature data for ORR on silver are very different depending on their authors [27–29]. Silver-surface state (surface oxide coverage) seems to affect the kinetics of the reaction. Thus, the influence of the prereduction was studied for silver nanoparticles (Ag/C) in 0.1 M sodium hydroxide at 25 °C in a pure oxygen atmosphere at 1.013×10^5 Pa. The starting oxygen reduction voltammetry potential was also studied: no effect was found in the range 0.1–0.0 V vs Hg/HgO. Conversely, the electrode prereduction changed the electrode behaviour towards ORR (Figure 2). The Tafel slope for low current density b_1 varied from -7.5×10^{-2} V dec^{-1} for non-prereduced Ag/C to -6.9×10^{-2} V dec^{-1} after one minute prereduction at -0.8 V vs Hg/HgO. Such Tafel slope variation related to silver-surface state was also mentioned by Sepa et al. [27]. Moreover, the current density decreased by more than an order of magnitude for industrial ORR potential values (around -0.1 V vs Hg/HgO) from non-prereduced to prereduced electrodes (Figure 2). Thus, the carbon-supported silver nanoparticle prereduction effect was negative for the ORR kinetics, and the following studies were carried out on non-prereduced electrodes. For comparison, bulk silver and platinum-based catalysts were also studied without any electrode prereduction.

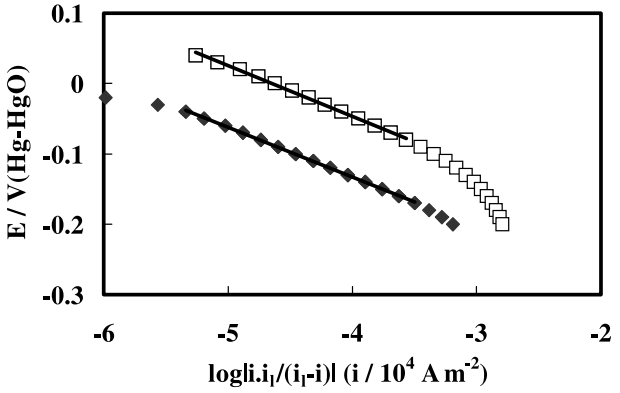

Fig. 2. Ohmic drop corrected Tafel slopes for oxygen reduction in 0.1 M NaOH at 25 °C on carbon-supported silver nanoparticles prereduced (♦) and non-prereduced (□); notation i_l for diffusion limiting current.

3.4. *Oxygen partial pressure (P_{O_2}) influence on oxygen reduction mechanism*

The ORR was studied in molar sodium hydroxide at 25 °C for two oxygen partial pressures: pure oxygen at atmospheric pressure ($P_{O_2} = 1.013 \times 10^5$ Pa) and *air* (20.9% O_2 + 79.1% N_2) at atmospheric pressure ($P_{O_2} = 2.12 \times 10^4$ Pa). As previously mentioned, the study only concerned b_1 and i_{-100}. No consequent Tafel slope variation towards oxygen partial pressure was found for ORR on Ag/C in molar sodium hydroxide at 25 °C (Figure 3). Moreover, for potentials close to −0.1 V vs Hg/HgO, the ratio i_{O_2}/i_{air} (Figure 4) was close to 4.8, corresponding to a first order kinetics with respect to oxygen partial pressure. Such behaviour implied the O_2-bond break after or during the ORR rate-determining step, according to one of the following three variants [6]:

$$O_2 \leftrightarrow (O_2)_{ads}$$

Variant I: $$(O_2)_{ads} + H_2O + e^- \rightarrow (O_2H)_{ads} + OH^- \quad \text{(rds)}$$

Variant II: $$(O_2)_{ads} + H_2O + e^- \rightarrow (O)_{ads} + (OH)_{ads} + OH^- \quad \text{(rds)}$$

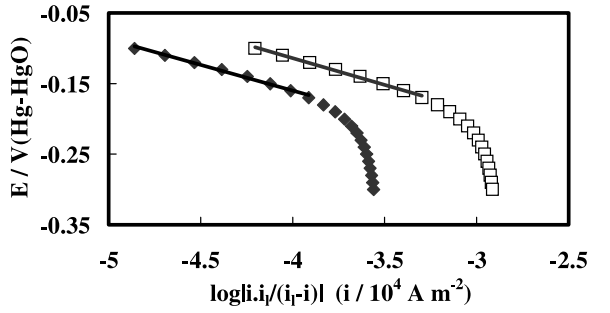

Fig. 3. Ohmic drop corrected Tafel slopes for oxygen reduction on carbon-supported silver nanoparticles in 1 M NaOH at 25 °C under air (♦) and oxygen (□) at 1.013×10^5 Pa.

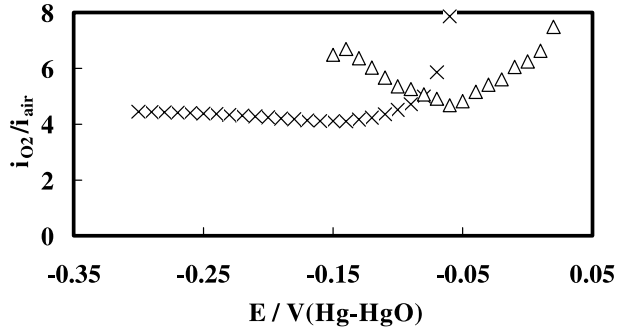

Fig. 4. i_{O_2}/i_{air} ratio against electrode potential for Ag/C (×) and Pt/C (△) active layer in NaOH 1 M at 25 °C.

Variant III: $$(O_2)_{ads} + e^- \rightarrow (O_2^-)_{ads} \quad \text{(rds)}$$

Besides, for high potential values (higher than −0.08 and −0.03 V vs Hg/HgO for Ag/C and Pt/C, respectively), the n increase resulted from a high relative error on current densities due to their low experimental values. Thus in molar sodium hydroxide at 25 °C, the ORR both on Ag/C, Pt/C and Pt, also in various alkaline media in that latter case [14], is first order kinetics towards molecular oxygen partial pressure, as already determined on Pt/C [6].

Considering the bulk Pt [14, 30, 31] and Pt/C (Figure 4) exhibited analogous behaviour towards oxygen partial pressure, it will also be considered that ORR on Ag has first order kinetics with respect to oxygen as already shown on Ag/C.

3.5. *Number of electrons exchanged per oxygen molecule*

3.5.1. *In 1 M sodium hydroxide at 25 °C*

Literature data assume a four-electron pathway for ORR on platinum catalysts in dilute alkaline media [1, 32, 33]. Experiments for confirmation were undertaken in 1 M sodium hydroxide at 25 °C, both on Pt and Pt/C.

Using the classical formula:

$$n = 4I_D/[I_D + I_R/N]$$

the knowledge of I_D and I_R, respectively, the RRDE disc and ring current, and N its collection efficiency, leads to the number of electrons exchanged per oxygen molecule, n. For Pt/C, n was almost equal to 4 in the scanned range of disc potential E_D (Figure 5). This result was also found on bulk Pt [14, 15]. It confirmed that ORR on platinum catalysts quantitatively leads to hydroxide ion formation in a dilute alkaline medium. Although no attempts have been undertaken on silver, it is probable that four electrons are also exchanged per oxygen molecule on this catalytic material, as reported in the literature. However, peroxide ion formation would vary with silver surface state and the electrolyte purity [34]. Moreover, both for silver and platinum, the catalyst ability to exchange four electrons per oxygen molecule is often coupled to that of peroxide chemical decomposition [7].

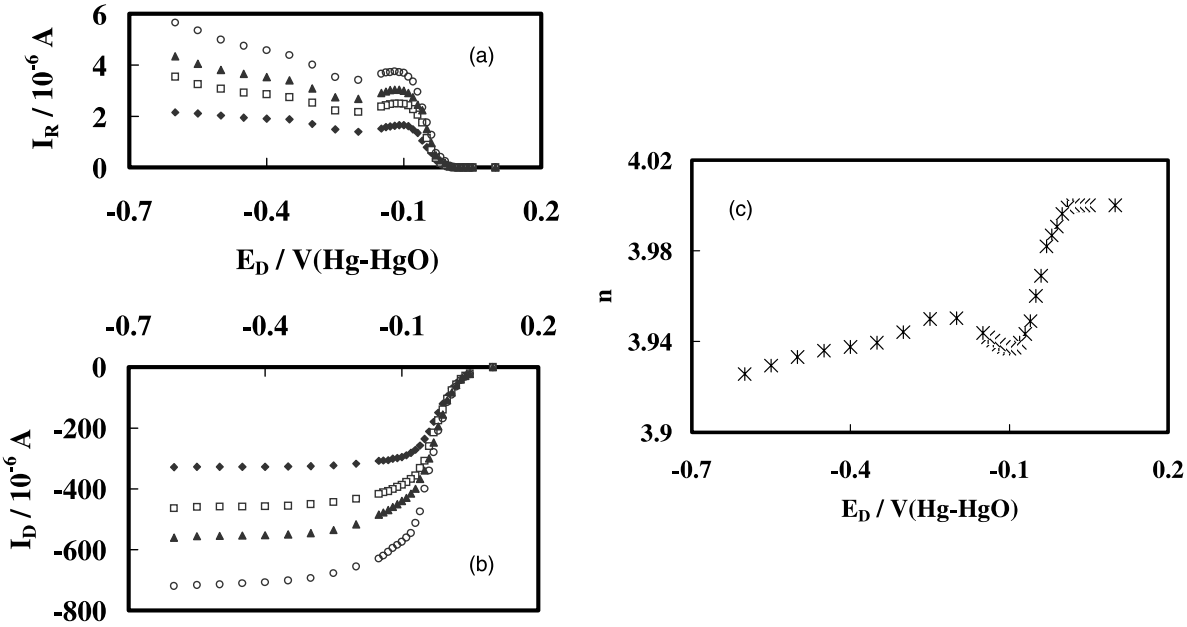

Fig. 5. I_R (a) and I_D (b) as a function of the disc potential E_D of a Pt/C–Pt RRDE for ORR in 1 M sodium hydroxide at 25 °C. Key: (♦) 42, (□) 84, (▲) 126, (○) 210 rad s^{-1}. (c) Corresponding number of electrons exchanged per oxygen molecule, *n*.

3.5.2. *In an industrial medium (11.1 M NaOH at 80 °C)* Determination of *n* on platinum catalysts in an industrial electrolyte revealed different behaviour for bulk polycrystalline and carbon-supported platinum. Whereas almost four electrons were exchanged on Pt/C, peroxide production on bulk Pt was not negligible (Figure 6). Platinum is an excellent peroxide ion chemical decomposition catalyst [4, 7]: the peroxide formed on Pt/C would be decomposed in the active layer where numerous platinum sites are available during their diffusion in the layer thickness. No peroxide ion is then detected on the platinum ring. This cannot happen on Pt and peroxide is detected massively on the RRDE ring. Thus, ORR for platinum-based active layer globally involves four electrons per oxygen molecule, as schematized below:

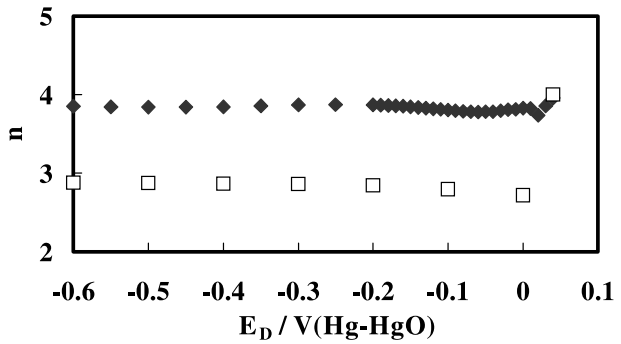

Fig. 6. Number of electrons exchanged per oxygen molecule (*n*) for ORR in 11.1 M sodium hydroxide at 80 °C on Pt/C (♦) and Pt (□).

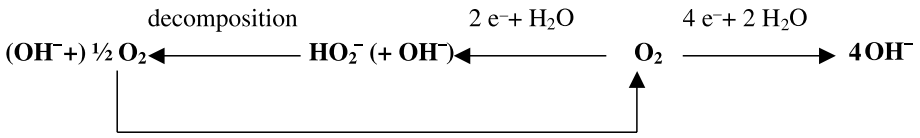

Because silver exhibits great catalytic activity towards peroxide ion decomposition [6, 7], the ORR on Ag/C also globally involves four electrons per oxygen molecule.

Finally, we consider that ORR on carbon-supported silver or platinum involves four electrons per oxygen molecule, even in 11.1 M sodium hydroxide at 80 °C, which is of great interest for the air cathode in brine electrolysis.

3.6. *Impedance study*

To decrease the diffusion effect, which is preponderant at low frequencies [35], porous electrodes with the same active layer as for RDE were prepared: Pt/C or Ag/C with PTFE. In the two cases, similar diagrams (Figure 7 for Ag/C) as for ORR on Pt/C in acidic medium [35] were obtained. The main feature is an inductive loop at low frequency [36], which characterizes a mechanism with two electrochemical steps [35], for example using variant I (cf. Section 3.4):

$$(O_2)_{ads} + H_2O + e^- \rightarrow (O_2H)_{ads} + OH^-$$

$$(O_2H)_{ads} + H_2O \rightarrow 3(OH)_{ads} \quad \text{(global chemical step)}$$

$$(OH)_{ads} + e^- \rightarrow OH^-$$

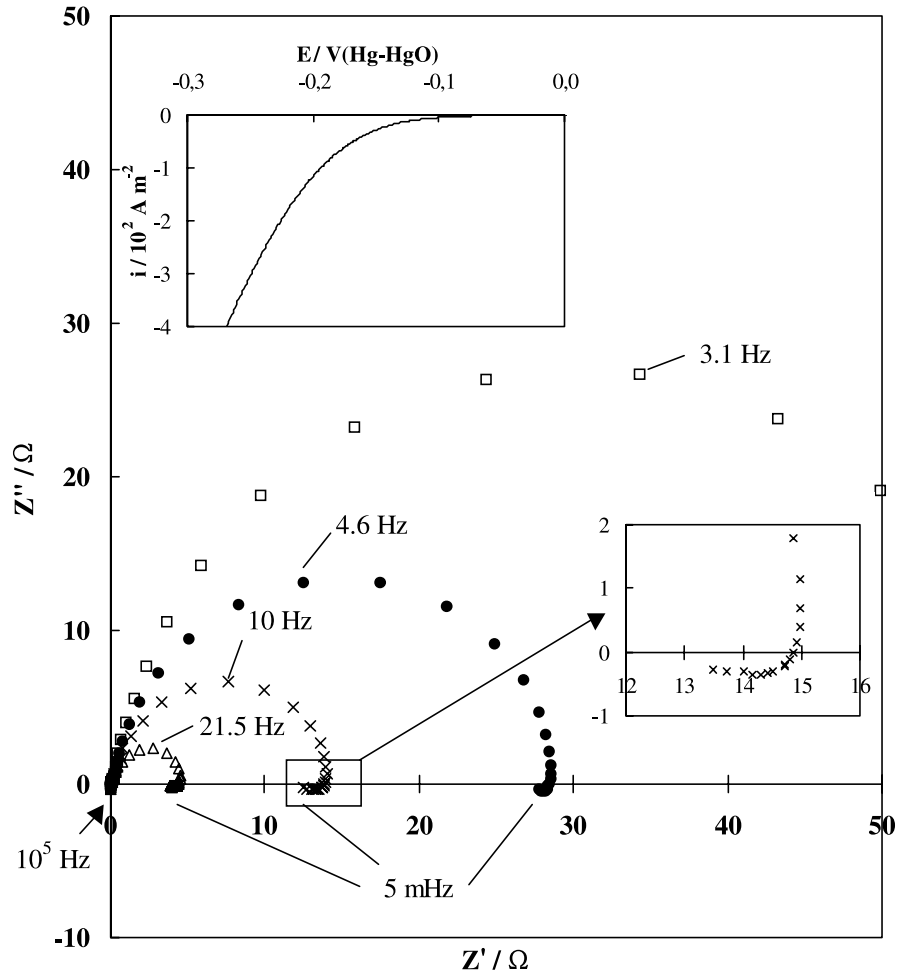

Fig. 7. Nyquist diagrams for ORR in an active layer Ag/C + PTFE (gas porous electrode) in 1 M NaOH at 25 °C for various potentials: −0.10 (□), −0.12 (●), −0.15 (×) and −0.18 V vs Hg/HgO (△).

In addition to this ECE mechanism, the following EEC mechanism cannot be excluded:

$$(O_2)_{ads} + H_2O + e^- \rightarrow (O_2H)_{ads} + OH^-$$

$$(O_2H)_{ads} + e^- \rightarrow O_2H^-$$

$$O_2H^- \rightarrow \frac{1}{2}O_2 + OH^-$$

It takes into account the possibility of a fairly fast O_2H^- chemical decomposition.

This impedance study is therefore consistent with the interpretation of the steady-state measurements.

3.7. *Temperature influence on the oxygen reduction reaction kinetics*

The impact of temperature variations on the ORR kinetics was studied for bulk Ag and Pt or nanoparticles, Ag/C and Pt/C, in 1 or 11.1 M sodium hydroxide in the range 10–80 °C.

3.7.1. *ORR on Ag and Pt*

Table 1 shows b_1, i_0 and i_{-100} variations with the temperature for ORR on bulk polycrystalline silver and platinum. b_1 slightly increased with temperature, in agreement with literature data [31]. i_{-100} (corrected by the oxygen solubility) also increased with temperature:

Table 1. ORR kinetic parameters on bulk silver (Ag) or platinum (Pt) in various sodium hydroxide solutions at various temperatures
Values reported to the reference oxygen solubility (in 1 M NaOH at 25 °C)

	$b_1/10^{-2}$ V dec^{-1}		i_{-100}/A m^{-2}		i_0/A m^{-2}	
	Ag	Pt	Ag	Pt	Ag	Pt
1 M NaOH (25 °C)	7.4	5.2	0.34	5.8	1.7×10^{-6}	6.9×10^{-6}
1 M NaOH (80 °C)	7.7	–	1.8	42	1.4×10^{-4}	–
11.1 M NaOH (80 °C)	*(4.4)*	6.9	20	39	*(1.4×10^{-6})*	1.2×10^{-3}

factors 5.3 and 7.2 were, respectively, found on Ag and Pt for a 25–80 °C temperature jump. Such values agree with the Geniès–Bultel survey [6], in which a factor 4 is found for i_0 in molar sodium hydroxide on Pt at 25 and 80 °C. The positive influence of temperature for the ORR kinetics on bulk Ag and Pt resulted in an increase in the kinetic constant k, whose expression varies as $\exp(-\Delta G_a/RT)$, with $\Delta G_a > 0$, assuming the Arrhenius law validity. The agreement between experiments and theory highlights the positive effect of temperature on ORR kinetics on bulk polycrystalline silver and platinum.

3.7.2. *ORR on Ag/C and Pt/C*

Table 2 shows b_1, i_0 and i_{-100} variations with the solution temperature and concentration for Ag/C and Pt/C. The experimental current densities were corrected for diffusion both in solution and in the active layer.

For Ag/C, b_1 decreased with increase in temperature. This variation, as opposed to that on bulk Ag, seemed nevertheless to indicate an improvement in the ORR kinetics with temperature. b_1 variation was, however, less characteristic of the ORR kinetics than the current density: b_1 determination depended on the potentials considered and was hindered by the existence of two Tafel slopes on silver as on platinum [37]. i_{-100}, whose determination was more straightforward and accurate, slightly increased with temperature, as for bulk Ag. This classical behaviour highlighted the improvement of the ORR kinetics with the temperature at −0.1 V vs Hg/HgO.

The variation of Pt/C kinetic parameters with temperature corresponded to that of bulk polycrystalline catalysts (increase of b_1 and i_{-100} values), even in high concentration sodium hydroxide solutions. This demonstrates the positive effect of a temperature increase for the ORR kinetics on Pt/C.

Finally, the ORR kinetic variation with respect to the medium temperature is in agreement with theory. In the range 10–80 °C, the higher the temperature, the faster the reaction both on carbon-supported nanoparticles and bulk polycrystalline silver or platinum.

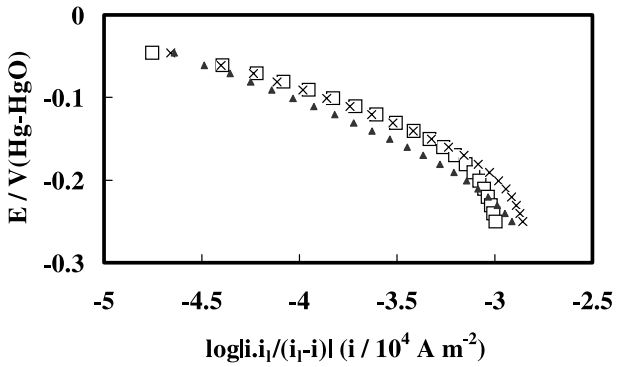

Fig. 8. Ohmic drop corrected Tafel slopes for oxygen reduction on carbon-supported silver nanoparticles in 0.1 M (▲), 0.5 M (□) and 1 M (×) NaOH at 25 °C.

3.8. *Influence of sodium hydroxide concentration on oxygen reduction kinetics*

ORR kinetics was studied on Ag/C in the range 0.1–1.0 M sodium hydroxide at 25 °C and on Ag, Pt or Ag/C and Pt/C in 1 M and 11.1 M sodium hydroxide solutions at 25 °C or 80 °C.

3.8.1. *Low concentration range (Ag/C)*

Figure 8 shows the Tafel slopes for oxygen reduction on Ag/C in 0.1, 0.5 or 1 M sodium hydroxide solutions at 25 °C. In the low concentration range, the ORR kinetics barely varied with sodium hydroxide concentration. The weak b_1 decrease with increase in hydroxide ion concentration (Table 2) may be attributed to an insufficient correction for diffusion in the active layer for the lowest concentrations, and can be considered insignificant. No concentration effect explained i_{-100} variations for sodium hydroxide concentration in the range 0.1–1 M. Such small variations (factor 2) are common for electrochemical kinetic parameters.

Finally, sodium hydroxide concentration in the range 0.1–1 M does not affect the ORR on Ag/C at 25 °C. This result was predictable considering the contradictory literature conclusions [30, 38].

3.8.2. *High concentration range (Ag/C, Pt/C, bulk Ag and Pt)*

For 1 M and 11.1 M sodium hydroxide concentration at 25 °C or 80 °C, sodium hydroxide concentration

Table 2. ORR kinetic parameters on Ag/C or Pt/C in various sodium hydroxide solutions at various temperatures
Values corrected by the diffusion in solution and in the active layer and reported to the reference oxygen solubility (in 1 M NaOH at 25 °C)

	$b_1/10^{-2}$ V dec^{-1}		i_{-100}/A m^{-2}		i_0/A m^{-2}	
	Ag/C	Pt/C	Ag/C	Pt/C	Ag/C	Pt/C
1 M NaOH (10 °C)	7.9	–	5.5×10^{-2}	–	4.8×10^{-7}	–
0.1 M NaOH (25 °C)	8.4	–	3.7×10^{-2}	–	4.2×10^{-7}	–
0.5 M NaOH (25 °C)	7.0	–	2.0×10^{-2}	–	1.4×10^{-7}	–
1 M NaOH (25 °C)	7.8	6.3	6.6×10^{-2}	8.9×10^{-1}	4.5×10^{-7}	3.9×10^{-7}
1 M NaOH (40 °C)	7.1	–	6.1×10^{-2}	–	1.4×10^{-7}	–
1 M NaOH (80 °C)	6.5	–	6.8×10^{-2}	–	4.8×10^{-8}	–
11.1 M NaOH (25 °C)	–	5.9	–	5.5×10^{-1}	–	9.6×10^{-8}
11.1 M NaOH (80 °C)	8.8	7.2	4.7×10^{-1}	1.1	3.1×10^{-6}	1.4×10^{-5}

variations affected the ORR kinetics more sharply, both on bulk Ag and Pt (Table 1) and Ag/C and Pt/C (Table 2). Moreover, platinum and silver catalysts behaved differently. A factor 11 for Ag and 7 for Ag/C was found for the ratio [i_{-100} (11.1 M)/i_{-100} (1 M)] at 80 °C: a concentration increase favours the ORR on silver. An ORR kinetics improvement with concentration was found neither for Ag/C in the low concentration range, nor in the literature. Conversely, the values 0.9 and 0.6, respectively, found for bulk Pt at 80 °C and Pt/C at 25 °C highlight the negative effect of concentration on platinum, which might originate from [26]:

(i) An ORR mechanism change (the ORR would involve 4 and 2 e^-, respectively, in low concentration sodium hydroxide and industrial solutions)
(ii) A platinum surface pollution increase, due to the impurities probably more present in industrial solution than in low concentration sodium hydroxide
(iii) A platinum oxygenated species coverage increase, resulting in an active area decrease, ORR rds occurring on metallic platinum and not on its surface oxides.

The first hypothesis is not relevant, as ORR in 11.1 M sodium hydroxide apparently involved four electrons per oxygen molecule both for Ag/C and Pt/C. No differences were found for ORR on Pt/C in various 1 M sodium hydroxide solutions (Suprapur, Merk; Normapur, Prolabo; Atofina), rendering improbable any influence of the impurities [26], discounting the second hypotheses. Only the third hypothesis should be taken into account. Whereas voltammograms under inert gas for bulk Ag (Figure 9) did not reveal any peak related to a surface oxide reduction in the ORR potential range ($E < 0$ V vs Hg/HgO), those for bulk Pt showed dramatic surface oxide coverage increase (Figure 10). A few interferences were observed, mainly on the 11.1 M NaOH at 80 °C curve for bulk Ag. The curve slope probably depends on the residual oxygen amount in solution, as would be the shift between the two curves. However, the only peak observed for potentials beyond 0.1 V vs Hg/HgO in 11.1 M sodium hydroxide at 80 °C is probably correlated to dissolution–deposition phenomena or oxidation–reduction at the silver surface. No surface oxide coverage increase with sodium hydroxide concentration is observed on silver. Oxygenated-species desorption phenomena are more classical on platinum. Figure 10 exhibited a reduction peak in the ranges (0; −0.3) and (0; −0.4) V vs. Hg/HgO in 1 M and 11.1 M sodium hydroxide solutions, respectively, for the same operation conditions used for Figure 9. This peak corresponds to the desorption of the oxygenated species formed at the starting potential (0.2 V in both cases) during 60 s. Its coulometry increased three times when the sodium hydroxide concentration varied from 1 to 11.1 M: the amount of surface oxide formed at the starting potential increases with sodium hydroxide concentration. Platinum surface oxide coverage at −0.1 V vs Hg/HgO was then higher in 11.1 M than in 1 M sodium hydroxide, which was not observed for

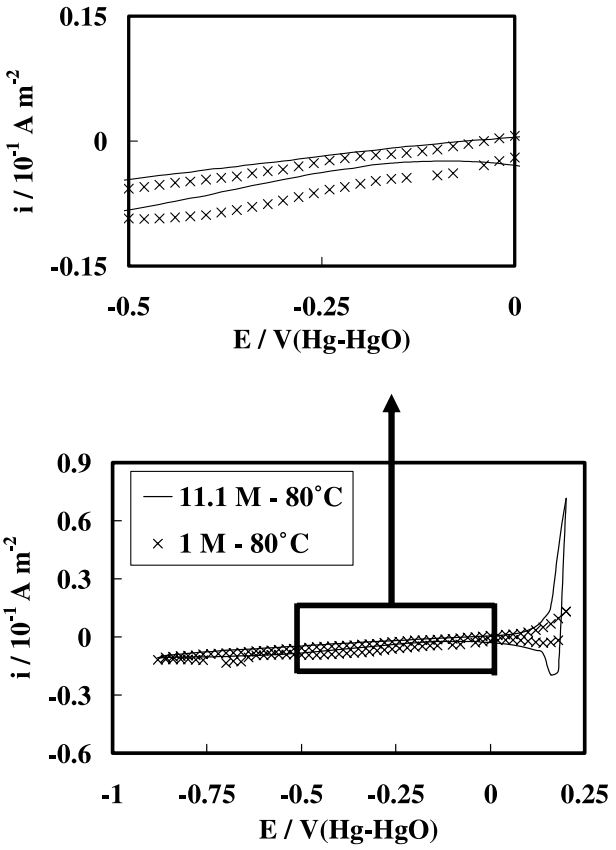

Fig. 9. Influence of the sodium hydroxide concentration on 2×10^{-2} V s^{-1} voltammograms shape under inert gas – Ag electrode at 80 °C: 1 M (×) and 11.1 M (——).

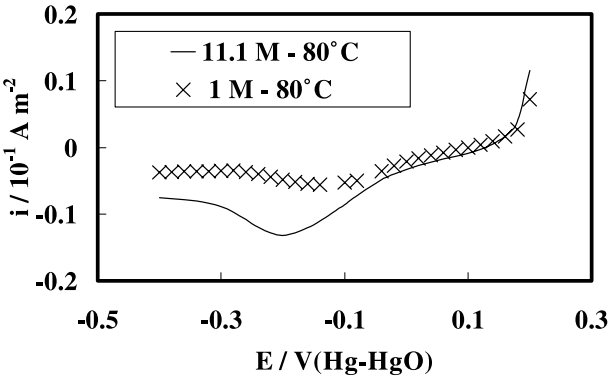

Fig. 10. Influence of the sodium hydroxide concentration on 2×10^{-2} V s^{-1} voltammograms shape under inert gas – Pt electrode at 80 °C: 1 M (×) and 11.1 M (—).

silver. Provided the ORR rds occurs on pure platinum and not on its surface oxides, the Damjanovic mechanism, the surface oxide coverage increase might explain the platinum catalytic activity decrease for higher sodium hydroxide concentration (moreover the mechanism probably involved two electrons per oxygen molecule on platinum surface oxides [37, 39]).

Finally, the platinum surface oxide (formed at a given potential) coverage increased with the sodium hydroxide concentration. Thus, the platinum apparent active area for the ORR r.d.s. (bare platinum) decreases, limiting the

reaction kinetics. Conversely, no increase in surface oxide coverage is found for silver and, unlike platinum, silver behaviour toward ORR is improved by an increase in sodium hydroxide concentration.

3.9. *ORR in an industrial electrolyte (NaOH 11.1 M at 80 °C)*

Bulk polycrystalline and carbon-supported silver or platinum behaviour were studied in 11.1 M sodium hydroxide at 80 °C. The corrected values for silver-based catalysts (Tables 1 and 2) showed the increase in reaction kinetics when the sodium hydroxide concentration and medium temperature both increased (from 1 M at 25 °C to 11.1 M at 80 °C). This result agreed with our previous results in dilute sodium hydroxide solutions: both effects were positive on silver. For platinum, the ORR kinetics improvement was much lower than for silver: the temperature had a positive effect and the sodium hydroxide concentration a negative one, the former being predominant.

Finally, the catalysts' hierarchy commonly admitted in dilute sodium hydroxide (1 M and below) is not true any more in an industrial electrolyte. Whereas platinum was about 10 to 20 times more interesting than silver (in term of i_{-100}) in molar sodium hydroxide at 25 °C, the gap between them did not exceed a factor 2–2.5 in an industrial electrolyte (Tables 1 and 2). This result was highlighted by the ORR current-potential curves for 11.1 M sodium hydroxide at 80 °C (Figure 11). The current densities were fairly similar on the whole potential range studied, with the Pt/C current being slightly higher than that of Ag/C: the current ratio did not exceed 2.5. Thus, Ag/C use is interesting in air–cathode in membrane brine electrolysis.

4. Conclusion

Platinum and silver catalysts, both bulk polycrystalline and nanodispersed on carbon, were studied in sodium hydroxide solutions. ORR kinetics first order towards oxygen was demonstrated on both bulk metals. The number of electrons exchanged per oxygen molecule was determined in 1 M at 25 °C and 11.1 M at 80 °C sodium hydroxide solutions. On nanodispersed catalysts, no differences were found between the two metals: four electrons were apparently exchanged in the volume of the active layer. The temperature effect, studied in the range 10–80 °C was positive: temperature increase favoured the ORR kinetics for all catalysts. The effect of sodium hydroxide concentration was only positive for silver-based catalysts, whereas it was slightly negative for platinum, even with correction from the oxygen solubility in the solution. Indeed, the increase in sodium hydroxide concentration favoured the ORR kinetics for silver and hindered that for platinum. Consequently, silver, which was less active than platinum in dilute sodium hydroxide (concentration below 1 M at 25 °C), became competitive in industrial brine electrolysis electrolyte (NaOH 11.1 M at 80 °C) even when the catalyst loading was similar (for Ag/C and Pt/C).

Finally, carbon-supported silver (Ag/C) and carbon-supported platinum (Pt/C) provide comparable behaviour in industrial brine electrolysis sodium hydroxide solution, and considering silver is about 100 times cheaper than platinum, Ag/C is a suitable catalyst to be used in an air-cathode in brine electrolysis.

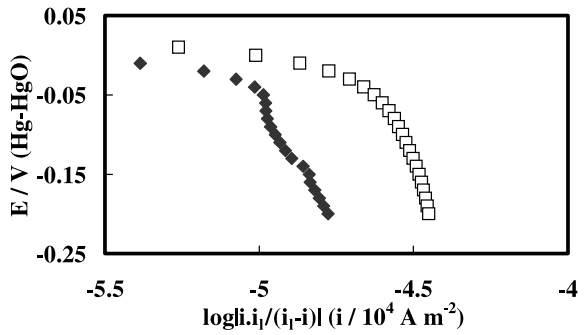

Fig. 11. Ohmic drop corrected Tafel slopes for oxygen reduction on carbon supported silver (♦) or platinum (□) nanoparticles in 11.1 M NaOH at 80 °C under oxygen at 1.013×10^5 Pa.

Acknowledgements

ATOFINA Research Centre (Centre de Recherche Rhône–Alpes, Pierre-Bénite, France) and the French Environmental Agency (ADEME) have supported this work.

References

1. L. Geniès, R. Faure and R. Durand, *Electrochim. Acta* **44** (1998) 1317.
2. J. Perez, A.A. Tanaka, E.R. Gonzalez and E.A. Ticianelli, *J. Electrochem. Soc.* **141** (1994) 431.
3. S.L. Gojkovic, S.K. Zecevic and R.F. Savinell, *J. Electrochem. Soc.* **145** (1998) 3713.
4. Y.F. Yang and Y.H. Zhou, *J. Electroanal. Chem.* **397** (1995) 271.
5. Y.F. Yang and Y.H. Zhou, *J. Electroanal. Chem.* **415** (1996) 143.
6. L. Geniès-Bultel, PhD thesis of INPG, Grenoble, France (1999).
7. H. Aikawa and J. Poblotzki, *Soda to Enso* **45** (1994) 85.
8. N. Furuya, O. Ichinose and A. Uchimura, Electrochemical Society Meeting, San Diego, CA, Abstract 785 (1998).
9. De Nora Permelec S.P.A., *German Patent*, DE 19 622 427 A1 (1996).
10. De Nora Permelec S.P.A., *German Patent*, DE 19 625 600 A1 (1997).
11. C.W. Walton and E.J. Rudd (Eds), 'Energy and Electrochem. Processing for a Cleaner Environment', Electrochemical Society Symposium, Pennington NJ, **97–28** (1997).
12. J.B. Goodenough, A. Hamnett, B.J. Kennedy, R. Manoharan and S.A. Weeks, *Electrochim. Acta* **35** (2000) 199.
13. M.P. Hogarth, J. Munk, A.K. Shukla and A. Hammett, *J. App. Electrochem.* **24** (1994) 85.

14. M. Chatenet, M. Aurousseau and R. Durand, *Indust. Eng. Chem. Res.* **39** (2000) 3083.
15. M. Chatenet, M. Aurousseau and R. Durand, *Electrochim. Acta* **45** (2000) 2823.
16. K. Jüttner and H. Siegenthaler, *Electrochim. Acta* **23** (1978) 971.
17. H. Siegenthaler, K. Jüttner, E. Schmidt and W.J. Lorenz, *Electrochim. Acta* **23** (1978) 1009.
18. H. Siegenthaler and K. Jüttner, *Electrochim. Acta* **24** (1979) 109.
19. E. Schmidt and H. Siegenthaler, *J. Electroanal. Chem.* **150** (1983) 59.
20. V. Daujotis and E. Gaidamauskas, *J. Electroanal. Chem.* **446** (1998) 151.
21. H. Kita, H. Nakajima and K. Hayashi, *J. Electroanal. Chem.* **190** (1985) 141.
22. G. Orozco, M.C. Perez, A. Rincon and C. Gutierrez, *Langmuir* **14** (1998) 6297.
23. E.R. Savinova, S. Wasle and K. Doblhofer, *Electrochim. Acta* **44** (1998) 1341.
24. E.R. Savinova, P. Kraft, B. Pettinger and K. Doblhofer, *J. Electroanal. Chem.* **430** (1997) 47.
25. O. Nekrassova, K. Tammeveski, M. Arulepp, T. Tenno, A. Rosental and V. Sammeslselg, ISE Meeting, Warsaw, Abstract 701 (2000).
26. M. Chatenet, PhD thesis of INPG, Grenoble, France (2000).
27. D. Sepa, M. Vojnovic and A. Damjanovic, *Electrochim. Acta* **15** (1970) 1355.
28. P. Fisher and J. Heitbaum, *J. Electroanal. Chem.* **112** (1980) 231.
29. P.K. Adanuvor and R.E. White, *J. Electrochem. Soc.* **135** (1988) 2509.
30. A. Damjanovic and V. Brusic, *Electrochim. Acta* **12** (1967) 615.
31. M.F. Weber, M.J. Dignam, Su-Moon Park and R.D. Venter, *J. Electrochem. Soc.* **133** (1986) 734.
32. A.J. Appleby and M. Savy, *J. Electroanal. Chem.* **92** (1978) 3351.
33. E. Yeager, *Electrochim. Acta* **29** (1984) 1527.
34. A.J. Appleby and F.R. Foulkes, '*Fuel Cell Handbook*' (Van Nostrand Reinhold, New York (1989), p. 384.
35. O. Antoine, Y. Bultel and R. Durand, *J. Electroanal. Chem.* **499** (2001) 85.
36. D.B. Zhou and H. Vander Porten, *J. Electrochem. Soc.* **145** (1998) 936.
37. N.M. Markovic, H.A. Gasteiger and P.N. Ross, *J. Phys. Chem.* **100** (1996) 6715.
38. M.R. Tarasevic, A. Sadkowski and E.B. Yeager, in B.E. Conway, J. O'M Bocris, E.B. Yeager and E.R. White (Eds), *Comprehensive treatise of Electrochemistry*, Vol. 7 (Plenum, New York, 1983), p. 301.
39. D.B. Zhou and H. Vander Porten, *J. Appl. Electrochem.* **26** (1996) 833.